

## Guided waves propagating in subducted oceanic crust

S. Martin and A. Rietbrock<sup>1</sup>

Institut für Geowissenschaften, Universität Potsdam, Potsdam, Germany

C. Haberland and G. Asch

GeoForschungszentrum Potsdam, Potsdam, Germany

Received 14 February 2003; revised 1 August 2003; accepted 12 September 2003; published 20 November 2003.

[1] We use guided waves traveling updip along the surface of the Nazca slab to image subducted oceanic crust at the Chile-Peru subduction zone. Observed *P* onsets of intermediate depth events near 21°S in northern Chile reveal waveguide behavior: with growing focal depth, low-frequency energy (<2 Hz) becomes more and more dominant, and higher frequencies arrive delayed, sometimes resembling two distinct phases. To explain the observations, we employ two-dimensional finite difference (FD) simulations of complete *P-SV* wave propagation along an updip profile of the subduction zone. The FD calculations shed some light on several basic issues regarding crustal waveguides. The development of guided waves dependent on event focal depth is simulated. Further, we show that the observed guided wave energy must decouple from the waveguide near 100 km depth to reach the deployed stations and that the decoupling process is related to variations in subduction angle. Simulations also yield constraints on source locations relative to the low-velocity structure. Finally, the frequency content of *P* onsets is used to constrain the thickness of the waveguide. The results indicate that a structure of <4.5 km average width and 7% low-velocity remains seismically slow compared to the surrounding mantle down to a depth of at least 160 km. The layer is interpreted as the unaltered lower part of the subducted oceanic crust, suggesting that complete eclogite transformation in the Chile-Peru subduction zone is unlikely to take place until beyond the volcanic front.

*INDEX TERMS:* 3210 Mathematical Geophysics: Modeling; 7220 Seismology: Oceanic crust; 7260 Seismology: Theory and modeling; 8150 Tectonophysics: Plate boundary—general (3040);

*KEYWORDS:* subducted oceanic crust, guided waves, FD modeling, low-velocity layer, Chile-Peru subduction

**Citation:** Martin, S., A. Rietbrock, C. Haberland, and G. Asch, Guided waves propagating in subducted oceanic crust, *J. Geophys. Res.*, 108(B11), 2536, doi:10.1029/2003JB002450, 2003.

### 1. Introduction

[2] The fate of subducted oceanic crust at intermediate depths is of main contemporary interest for understanding the subduction processes and, in particular, the origin of intermediate depth earthquakes [Meade and Jeanloz, 1991; Abers, 2000; Yuan *et al.*, 2000]. Seismic waves from intraslab earthquakes that probe the seismic velocity structures of slabs are a valuable source of information on the mineralogical and thermal structure of subducted lithosphere [e.g., Davies and McKenzie, 1969; Kirby *et al.*, 1996]. Seismic wave anomalies are used to infer seismic velocity structure of subducted lithosphere and ultimately information on slab mineralogy [Mitronovas *et al.*, 1971].

[3] Velocity contrasts are derived from observations of a variety of seismic signals that are influenced by the

subducted plate. Travel times, for example, are easy to measure but only yield average velocities along ray paths [e.g., Fukao *et al.*, 1978]. Detailed velocity structure within the slab that gives evidence for mineralogical phase changes can thus not be imaged [Mitronovas *et al.*, 1971].

[4] Another widely used technique employs converted waves caused by the slab surface or layering within the subducted lithosphere. Helffrich and Abers [1997], for example, employed converted waves to investigate a low-velocity layer at the eastern Aleutian subduction zone. Studies at the Chile-Peru subduction zone in the western central Andes inferred a similar layer up to depths of 120–160 km from *P-S*-converted waves [Yuan *et al.*, 2000; Bock *et al.*, 2000]. The resulting velocity contrast is 15% with a thickness of 5–10 km. Likewise, investigations at the northeast Japanese subduction zone found undulating velocity contrasts between the accretional wedge and subducted crust at various depths which are interpreted as evidence of chemical phase changes of the gabbroic subducted crust [Snoke *et al.*, 1978; Helffrich, 1996].

<sup>1</sup>Now at Department of Earth and Ocean Sciences, Liverpool University, Liverpool, UK.

[5] Last, subducted lithosphere not only causes converted seismic body waves, but also can act as a seismic waveguide for up dip and along-strike signals of intraslab events. These signals provide the longest interaction times within the slab and thus yield potentially large slab related signals. The waveguide causes distortion in pulse shape and differences in long- and short-period energy arrival times.

[6] Among the mentioned methods, guided waves is one that is directly linked to the existence of layered structures such as subducted crust. A more or less continuous layering is a prerequisite for the occurrence of guided waves [Abers and Sarker, 1996; Abers, 2000]. Furthermore, studies on fault zones have shown so far that occurrence, pulse shapes and frequency content of guided waves are directly related to parameters such as layer thickness, length of the waveguide structure and source location in relation to the layer [Li and Vidale, 1996; Igel et al., 1997; Ben-Zion, 1998; [M. Fohrmann et al., Guided waves from sources outside faults: An indication for shallow fault zone structure?, submitted to *Pure and Applied Geophysics*, 2002, hereinafter referred to as Fohrmann et al., submitted manuscript, 2002].

[7] The first successful studies in subduction zones were undertaken for high-velocity structures, often modeling the whole slab as a high-velocity layer [e.g., Barazangi et al., 1972]. Observations at the Kermadec subduction zone gave proof that thinner layering also results in frequency effects. High-frequency phases were observed prior to low-frequency onsets at stations in New Zealand. This is explained by introducing a thin (8–10 km) high-velocity layer (5% faster than surrounding mantle) on top of the Kermadec plate [Ansell and Gubbins, 1986; Van der Hilst and Snieder, 1996].

[8] In accordance with investigations utilizing converted waves, the Japanese subduction zone, which has so far been investigated the most, features a low-velocity layer that causes guided wave effects. *P* onsets show low frequencies arriving faster than high frequencies. Studies on the crustal waveguide in the Philippine plate subducting beneath southwest Japan concluded that the wave guide was <10 km thick and that  $V_p$  equals 7 km/s for earthquake sources down to focal depth of 50–60 km [Fukao et al., 1983; Hori, 1990; Oda et al., 1990]. As these velocities were indistinguishable from those for oceanic crust beneath ocean basins, the waveguide was identified as gabbroic crust that survived untransformed to a depth of 50–60 km. In the Pacific plate subducting beneath northeast Japan, the low-velocity crustal channel persists to depths of 75–150 km, and its thickness is estimated to be about 5 km [Matsuzawa et al., 1986; Hurokawa and Imoto, 1992; Iidaka and Obara, 1993]. Since change in temperature cannot cause the appropriate velocity contrasts [e.g., Helffrich, 1996], it is likely, that a layering persists to greater depths than those reached beneath the volcanic arc. Recently, low-velocity layers were postulated for most of the subducted slabs in the north Pacific region down to depths of 100–250 km by evidence from guided waves [Abers, 2000].

[9] This study is motivated by the mentioned results at other subduction zones and promising observations from intraslab events at stations of the ANCORP'96 seismic network located between 21° and 24°S in northern Chile [Rietbrock et al., 1997].

[10] Typically, the observation of guided waves is restricted to the case of receivers situated within or close

to the waveguide rather than complex geometries including receivers at greater distances to the low-velocity layer [Ben-Zion et al., 2003]. Therefore we will address simple, but crucial questions regarding the potential of guided waves to examine layering of subducted lithosphere: (1) Under which circumstances does guided wave energy actually leave the waveguide structure and is observable at surface stations? (2) Which restrictions on source locations are required to have guided wave energy enter the low-velocity structure? (3) Do distorted *P* onsets allow estimates of structural parameters of the low-velocity zone? Ultimately, we infer under which circumstances guided wave energy from a low-velocity layer on top of the Nazca plate at the Chile-Peru subduction zone is observable in *P* onsets.

[11] We calculate complete *P-SV* wave propagation for a two-dimensional (2-D) cross section through the Chile-Peru subduction zone utilizing finite difference (FD) simulations. This allows us to compare directly pulse shapes and frequency content (up to 8.5 Hz) of collected data with synthetics for different slab geometries and internal structures. The FD calculations allow a much more direct approach to the problem than analytical guided wave solutions which are feasible for SH waves and plane layers only. Furthermore, the FD approach allows to investigate the decoupling process of guided waves from laterally inhomogeneous waveguide structures.

## 2. Data and Observations: Distorted Arrivals at ANCORP Station AER

[12] Data used come from the ANCORP'96 campaign that was undertaken during November 1996 to March 1997 in northern Chile between 23°–20.5°S and 70°–66.5°W [Rietbrock et al., 1997]. The ANCORP temporary seismic network consisted of 32 short-period stations equipped with Mark L-4A-3D sensors.

[13] A subset of stations (BOS, AER, VOL, CHG; see Figure 1), all located close to 69° ± 0.2° longitude, show distorted *P* wave first arrivals, sometimes resembling two distinctive phases. This work focuses on the data recorded at station AER, where the effect is most pronounced and the noise level is low. Events were selected from the latitude-longitude box 23.88°–21.95°S and 69.05°–66.29°W. They cover a range of focal depths from 70 to 300 km and form an up dip section centered around station AER (Figure 1).

[14] *P* waveforms in seismograms recorded at AER can be classified into two groups. A clear, impulsive onset is typical for the recorded shallow earthquakes (focal depth <110 km). In contrast, the *P* onset of earthquakes with greater focal depth (>140 km) at AER has low frequencies that form the early part of an extended wave train rather than a sharp onset (Figure 2).

[15] Offset was removed, and the data were band-pass-filtered (0.5–8.5 Hz). During the ANCORP'96 campaign, 48 events located deeper than 110 km were recorded at station AER. Forty-five of these 48 events show remarkably strong low-frequency energy arriving prior to higher frequencies. The effect is particularly strong for deeper events with larger hypocentral distances. A selected subset of seismograms representing different event depth illustrates the dependency on source location (Figure 3a). A relative increase of low-frequency energy with focal depth is evident

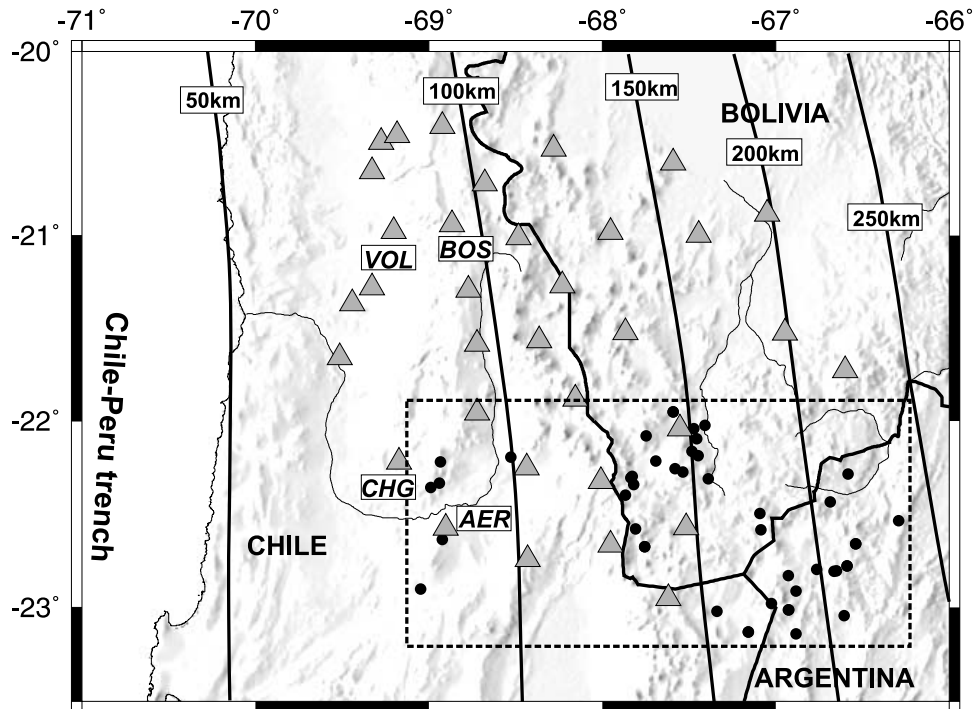


**Figure 1.** Map of the ANCORP'96 temporary seismic network consisting of 32 short-period stations (triangles) equipped with Mark L-4A-3D sensors. Solid lines represent depth contours. The dashed line contains events (dots) recorded at station AER forming an updip section centered at 22.58°S. The events were located by *Rietbrock et al.* [1997] using a local earthquake tomographic method.

from visual assessment. For one of the deepest events high-frequency energy ( $>5$  Hz) arrives up to 1.0 s later than energy below 2.5 Hz (compare Figure 3a). This suggests that slab structure is responsible for the effect. Figure 3b compares the summed up spectra of all events located above 110 km and below 140 km respectively. Only the latter spectrum exposes a clear peak around 2 Hz, while sources above 110 km lack this low-frequency energy. At the same time, the peak frequency of low-frequency energy for events located deeper than 140 km does not shift systematically precluding a pure attenuation effect.

### 3. Finite Difference Modeling of Waveguide Effects

[16] To gain an inside view of the mechanism underlying this systematically distorted pulse shapes, a numerical simulation of the wave propagation seems best suited. It is, however, a demanding task to simulate body waves with frequencies as high as 8.5 Hz that propagate hundreds of kilometers in a laterally inhomogeneous medium. An efficient, easy to parallelize, grid based finite difference technique was chosen to calculate complete  $P$ - $SV$  wave propagation within a 2-D depth section of the subducting Nazca slab.

[17] The elastodynamic equation of motion is expressed in terms of velocity and stress. Our approach uses a fourth-order staggered grid finite difference scheme as proposed by *Virieux* [1984, 1986]. The method is well suited for the challenge of simulating wave propagation up to high frequencies in large media (330 km  $\times$  260 km) including complicated boundaries. Furthermore, the model space can

easily be distributed on parallel computers. Since we are interested in frequency effects, special care must be taken to prevent numerical dispersion that would distort frequency content of guided waves. The efficient staggered grid method allows a fine discretization of the model while the cost of computing stays low. In the finite difference calculations, grid spacing is as little as 40 m, the time increment is only 0.0027 s. Thus even the highest frequencies of  $S$  waves are covered with 12 points per wavelength and

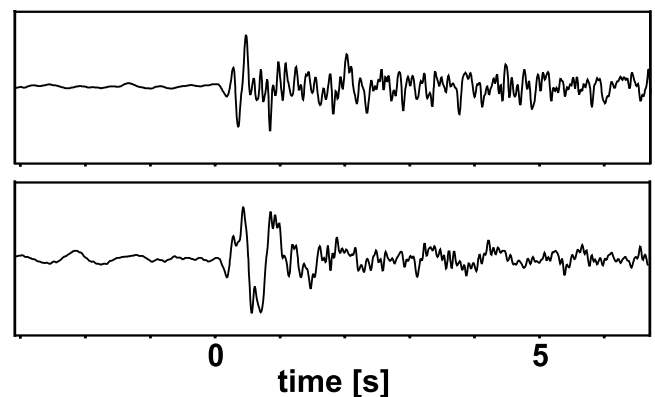


**Figure 2.**  $P$  onsets at station AER aligned on first arrivals and plotted proportional to ground displacement. Data are band-pass-filtered between 0.5 and 8.5 Hz, and amplitudes are normalized. (top) Event at 80 km focal depth (26 km epicentral distance) located close to station AER (see Figure 1). (bottom) Distorted  $P$  onset (focal depth 190 km, epicentral distance 167 km).

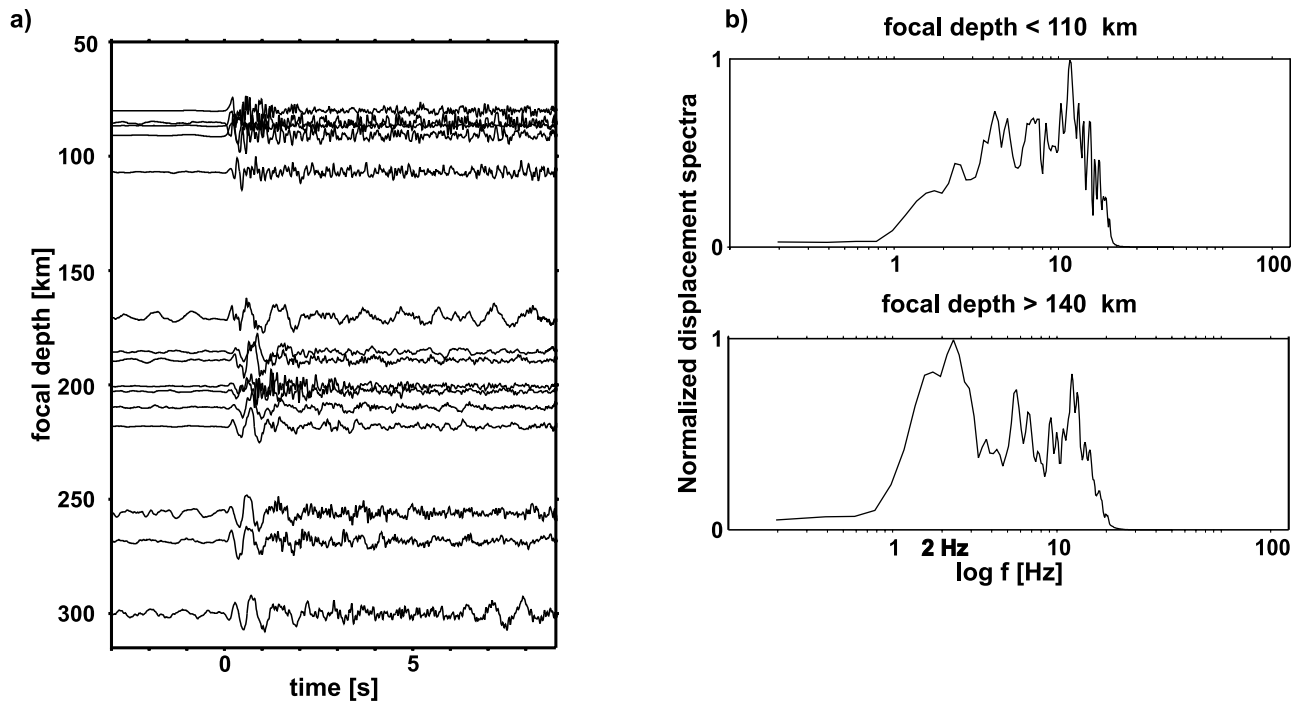


**Figure 3.** (a) Aligned  $P$  onsets of selected events recorded at station AER plotted by focal depth (for further explanations see Figure 2). (b) Stacked displacement spectra of onsets (first 2 s) of all events contained in the updip section (see Figure 1) with focal depth  $< 110$  km and  $> 140$  km, respectively.

numerical dispersion stays well below 0.5% [Levander, 1988].

[18] The scheme is rounded out using the planar free surface condition given by, e.g., Levander [1988], that employs a zero stress formulation to produce accurate and numerically stable surface reflections and  $P$ - $SV$  conversions. In order to excite guided waves within a broad frequency range, we use a delta impulse as source wavelet in conjunction with subsequent low-pass filtering (8.5 Hz). The artificial edges of the model are damped by simple exponential terms [Randal, 1989]. Because of hardware limitations, simulations of the given size, were, up to now, extremely cost intensive if not impossible to undertake. Today the scheme can be run on a LINUX cluster with 16 knots (1 GHz Pentium III) within 16 hours real time.

## 4. Excitation of Guided Waves and Dependencies on Structural Parameters

### 4.1. Guided Waves: Effects and Prerequisites

[19] Understanding and using the available data require a basic knowledge of waveguide phenomena. Any continuous layered structure that is slow compared to bounding media can act as a waveguide provided no large heterogeneities are present. Scales of layer thickness range from meters to tens of kilometers, dependent on the frequency range under observation. This structure causes, for certain source-receiver configurations, internally reflected waves that produce prominent interference patterns called guided waves. The effect is most pronounced for shear energy but does also occur for  $P$  waves. In this case, trapping of energy is less efficient and energy is leaking into the surrounding host rocks ( $P$ - $SV$ -converted waves originating at the interfaces of the low-

velocity structure). The first studies to utilize the effect for  $P$  and  $S$  waves in the context of tectonic faults are probably those of Fukao *et al.* [1983] and Hori *et al.* [1985].

[20] The dispersion properties of guided waves are such that the lowest frequencies propagate along the structure with velocities similar to  $P$  velocities of surrounding host rocks, while higher-frequency energy arrives later, dependent on structural parameters [Li and Leary, 1990]. The pulse shape and the frequency content of the resulting wave train is ultimately dependent on the material parameters and geometry of the waveguide structure. The interference pattern controlling the waveform character changes with the number of times the waves are reflected internally in the waveguide structure [Ben-Zion, 1998]. In particular, a minimum number of internal reflections is a prerequisite to perceive the interference pattern as a continuous dispersive wave train rather than separate phases. For given velocity contrasts, the number of reflections increases with propagation distance along the structure, and it decreases with the thickness of the structure.

[21] Thus occurrence of guided waves is restricted by a lower limit of propagation distance and an upper limit of waveguide thickness. In addition, observed motion is a strong function of relative lateral position of the source and lateral receiver coordinates. Finally, low-quality factors modify the dominant period and overall duration of the guided waves considerably [Ben-Zion, 1998].

[22] Within the context of the Chile-Peru subduction zone, we are able to utilize mineralogical interpretations to constrain velocity contrasts and studies of attenuation tomography give information on average quality factors. Thus geometry of the subducting slab along with receiver position, propagation length of signals along the layer

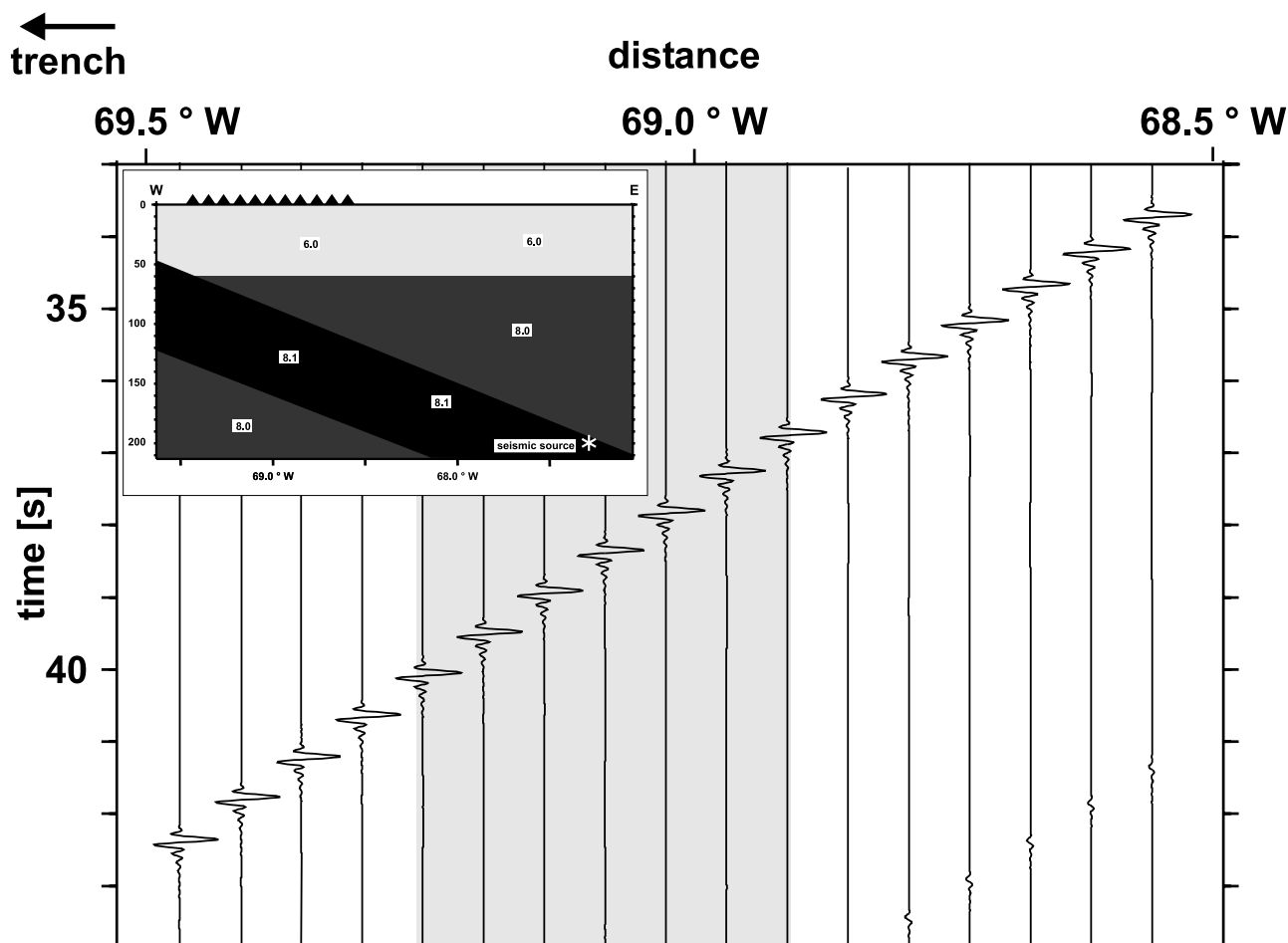


**Figure 4.** Velocity model (insert) and resulting seismogram section for an homogeneous slab of 1.25% increased velocity compared to continental mantle. Labels in the insert indicate  $P$  velocities. Synthetics are impulse responses proportional to ground displacement and low-pass-filtered with 8.5 Hz. The shaded area in the seismogram section marks the longitude range of ANCORP stations exposing distorted onsets.

(i.e., focal depth), thickness of subducted crust and the source position relative to the layer will be the parameters investigated.

## 4.2. Results

### 4.2.1. Slab Structure and Occurrence of Guided Waves

[23] We aim to reproduce the observed effect in principle, utilizing a velocity model that only contains the basic features common along the extent of the subduction zone from surface to intermediate depth. The basis is a simplified sketch of the subducted slab, deduced from refraction seismic studies [Lessel, 1997; Patzwahl, 1998] and works of Bock *et al.* [2000] and Yuan *et al.* [2000] using  $P$ s converted waves. Seismic velocity contrasts between continental mantle and slab surface in northern Chile could be traced down to depth of 160 km, while the oceanic Moho that delineates the subducted crust is visible down to 120 km. Continental crust is assumed to extend down to 60 km with an average  $P$  velocity of 6.0 km/s. Mantle  $P$  velocities at depth greater than 60 km are averaged to be 8.0 km/s, the subducted material of the relatively young Nazca plate appears only slightly faster (8.1 km/s). If subducted crust persists as a partially eclogized layer on

top of the slab surface,  $P$  velocities of 7.5 km/s are expected [Helffrich *et al.*, 1989; Hacker *et al.*, 2003a, 2003b]. The average subduction angle at latitude 21°S down to 300 km depth was inferred from the works of Graeber [1997] and Rietbrock *et al.* [1997] to be 30°. In our simulations we inserted a simple, if unrealistic, explosive source. The simulation of complete  $P$ - $SV$  wave propagation within a laterally inhomogeneous velocity model results in complicated seismogram sections. We therefore find it helpful to exclude influences of source functions and mechanisms from our investigations, allowing an unobstructed look at structural parameters of the waveguide.

[24] In advance of simulations that include a low-velocity layer, the wave field resulting from an unstructured subducted slab was inspected. The reference model includes a homogeneous slab of 1.25% higher velocity than the host rocks. The seismogram section of an event at 200 km focal depth located 5 km below the slab surface is depicted in Figure 4. No low-frequency energy emerges.

[25] The simplest structure to produce the observed low-frequency onsets is a planar low-velocity layer in an otherwise homogeneous medium such as slow subducted crust surrounded by faster mantle rocks. Therefore the first

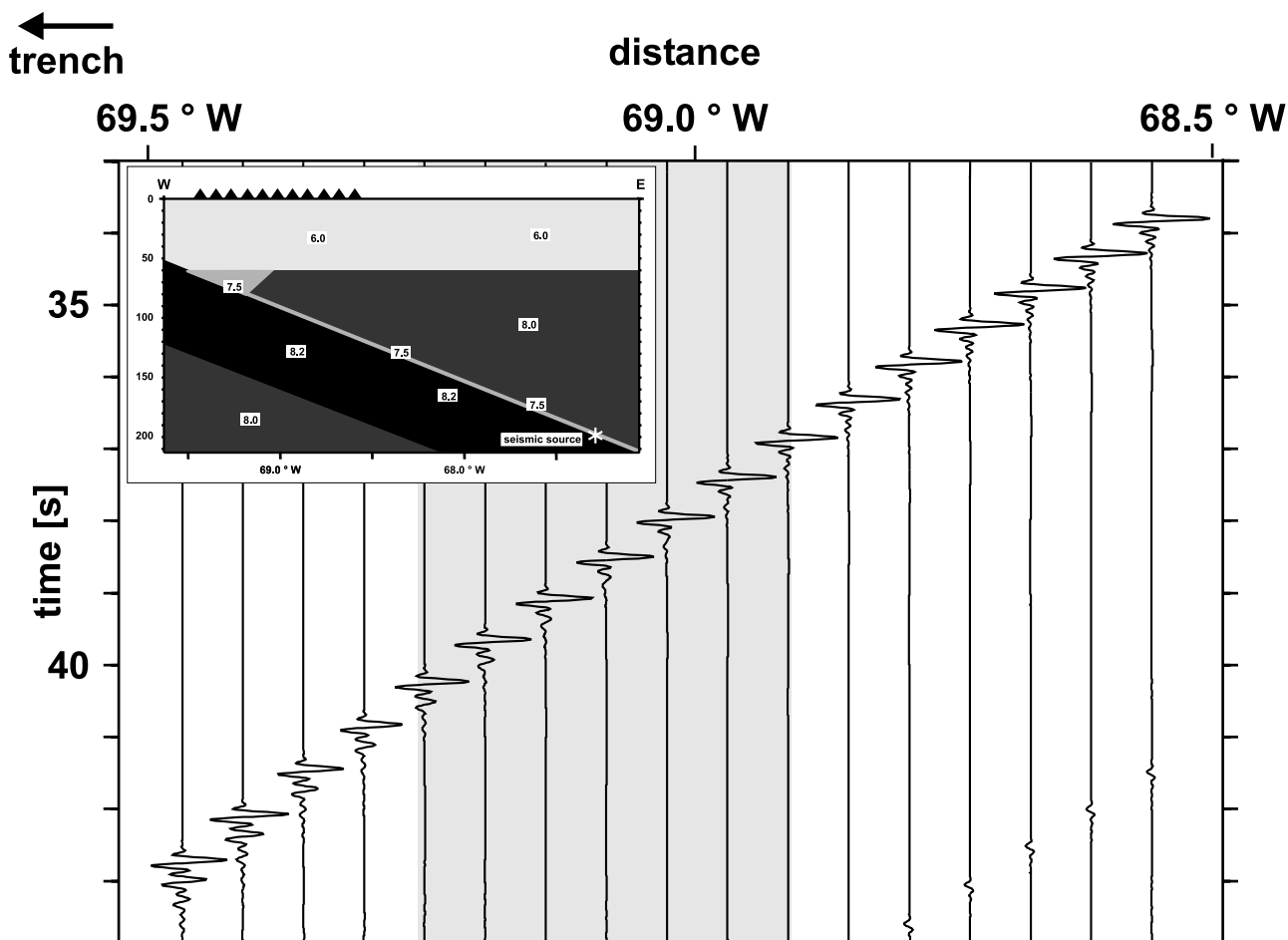


**Figure 5.** Velocity model (insert) and resulting seismogram section for a straight slab structure with a layer of 7% low velocity relative to continental mantle and 3 km width at its top. The shaded area marks the longitude range of ANCORP stations exposing distorted onsets. For further explanations, see Figure 4.

approach uses a model that is reduced to these three components. While guided waves begin to develop right from the start of their journey through the slab, the point of occurrence of guided wave energy at the surface is assumed to be determined mainly by the velocity structure above 100 km depth. Various studies on fault zone waves were already dedicated to the issue. Under which circumstances do guided waves leave the wave guide and can be observed outside of it? It has been shown that a maximum of guided wave energy is observed within and directly above a vertical low-velocity layer. With increasing distance from the layer, amplitudes decay rapidly [Igel *et al.*, 1997].

[26] A zone of transition below the receiver line in the continental mantle was assigned the same seismic velocities as the low velocity layer. The transition zone was placed at a depth of 80 km, where studies suggest the same velocities for subducted lithosphere and mantle [ANCORP Working Group, 1999] (model, see insert of Figure 5).

[27] To restrict the range of layer thickness and source location to those values that produce a maximum in guided wave energy within the desired frequency range (<5 Hz), spot checks were undertaken for a range of layer thicknesses (1–10 km) and source locations relative to the low-velocity

layer (ranging from 10 km below the subducted crust to sources located in the center of the subducted crust). Focal depth was 200 km, and the seismic velocity contrast toward continental mantle was kept at a constant of 7%. The strength of guided wave energy at a receiver located in the center of the layer was used as a criterion to estimate an upper limit for the layer thickness and ideal values for source location. In accordance with studies carried out for planar, vertical low-velocity layers [Igel *et al.*, 1997], the waveguide effect was most pronounced for sources located within the layer. A closer look at the effects of source positioning will be taken in section 4.2.4. The tests also indicated that for velocity contrasts <10% and the given focal depth, low-velocity layers thicker than 5 km do not cause sufficient internal reflections for the development of a guided wave train.

[28] Using maximum amplitudes and frequency content of guided waves as a measure [Igel *et al.*, 1997; Ben-Zion, 1998], the starting parameters for further simulations were set to 3-km layer thickness for a contiguous layer of 7% reduced velocity. The source at 200 km depth was located at a 0.3 km distance from the oceanic Moho inside the low-velocity layer.

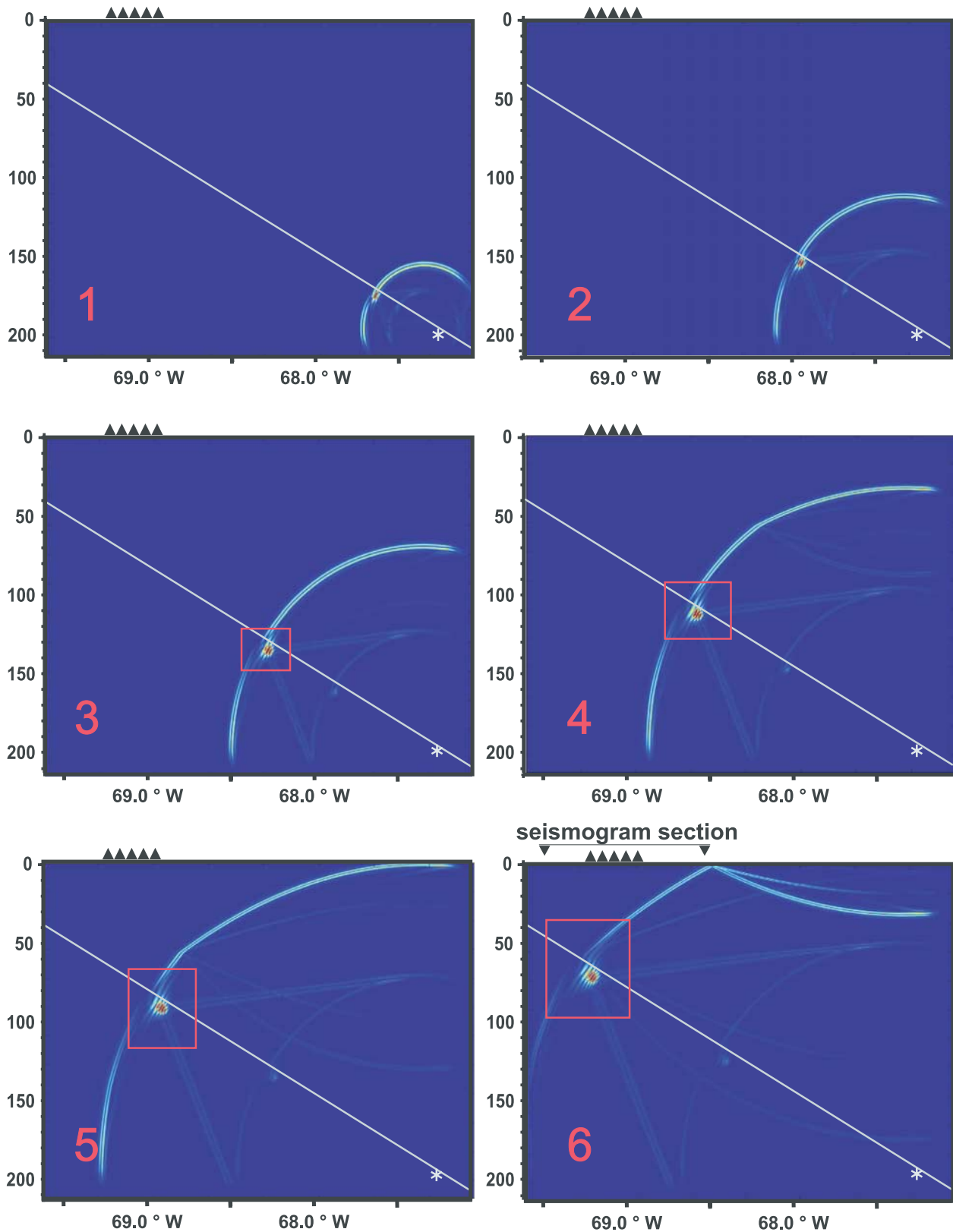


**Figure 6.** Snapshots of root-mean-square ground velocity of 2-D  $P$ - $SV$  wave propagation (velocity model see Figure 5). The gray line marks the slab surface, the red frame highlights the guided waves traveling along the slab surface. Solid triangles indicate receiver positions, and source position is indicated by asterisk.

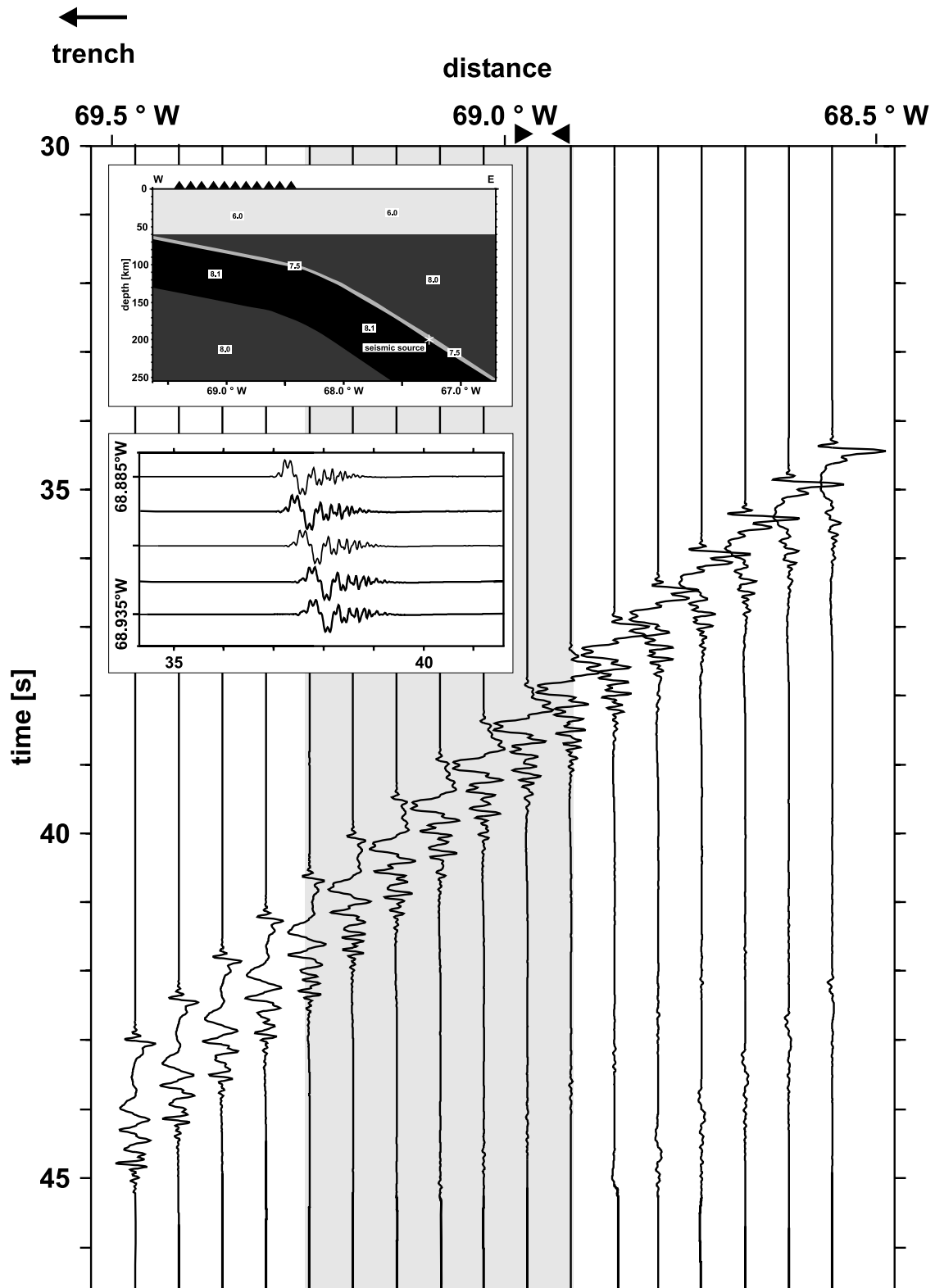


**Figure 7.** Seismogram section for a bend slab structure with a layer of 7% slow velocity and 2 km width at its top. The shaded area marks the longitude range of ANCORP stations exposing distorted onsets. Top insert is the velocity model including hypocenters after *Graeber* [1997] and *Rietbrock et al.* [1997] (black dots). Bottom insert shows enlargement of receivers located around 68.91°W (station AER).

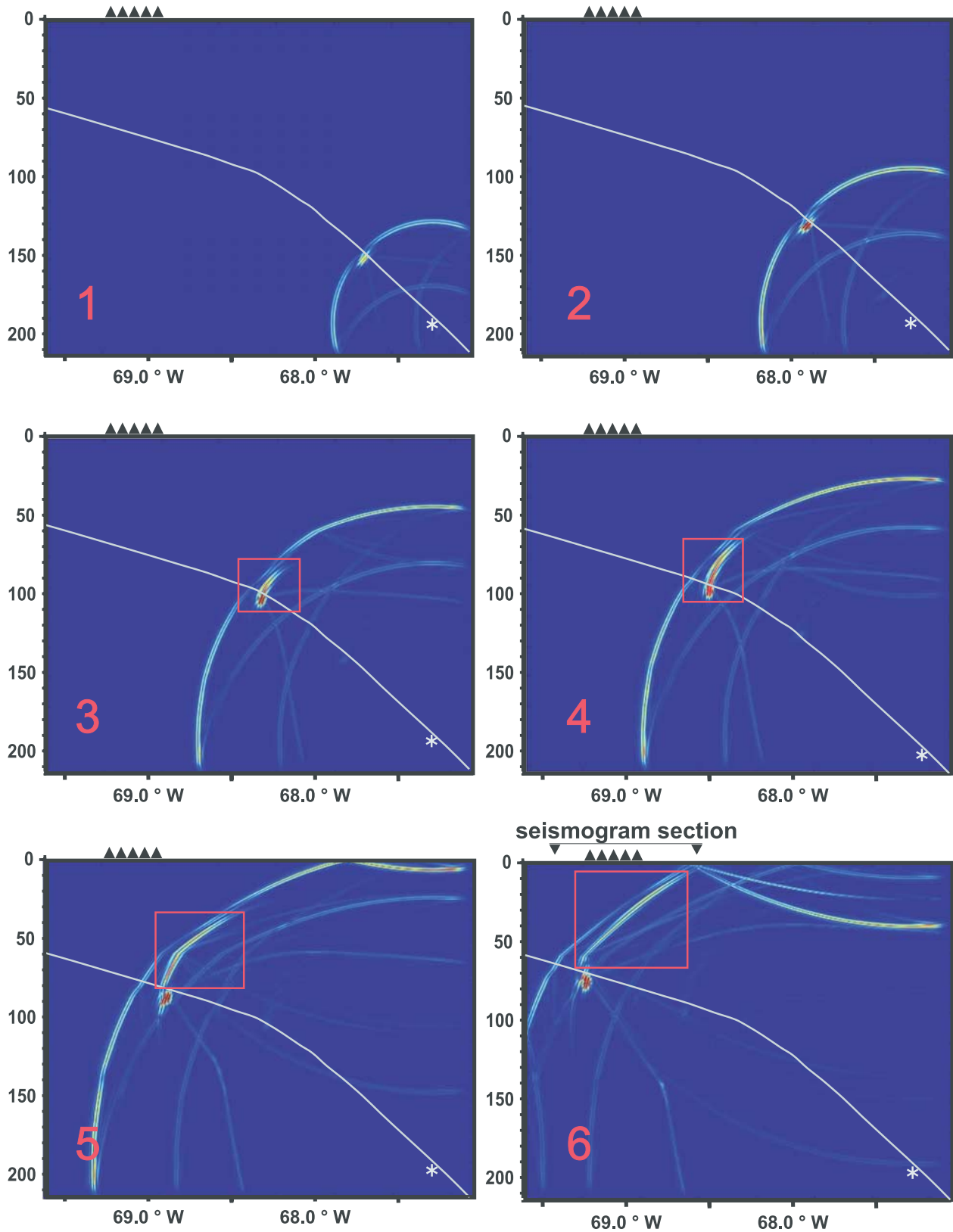


**Figure 8.** Snapshots of root-mean-square ground velocity of 2-D *P-SV* wave propagation (velocity model see Figure 7). The gray line marks the slab surface, the red frame highlights the parts of guided wave energy decoupling from the low-velocity layer. Solid triangles indicate receiver positions, and source position is indicated by asterisk.

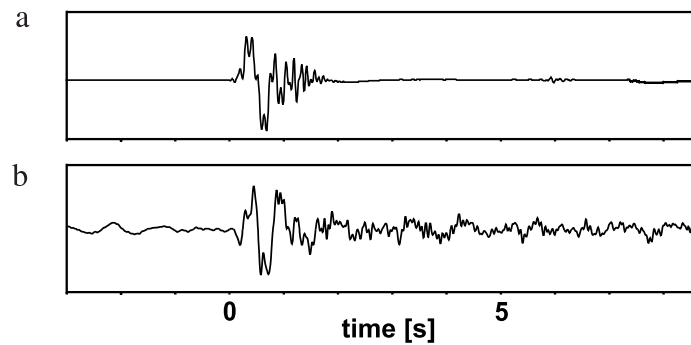


**Figure 9.** Aligned  $P$  onsets (displacement seismograms, low-pass-filtered with 8.5 Hz). (a) Synthetic signal resulting from the bent slab model (see insert of Figure 7) (receiver position  $68.9^\circ\text{W}$ ). (b) Observed signal for comparable hypocentral distance and receiver position (station AER).

[29] The receiver line of Figure 5 shows displacement seismograms starting roughly 90 km inland from the coast line. Guided wave energy does not appear anywhere near the stations of the ANCORP network at the free surface. However, snapshots of the wave field show the development of a guided wave train with strong amplitudes propagating upward along the slab surface (Figure 6). Considerable guided wave energy builds up, but the waves continue to travel trenchward with the same slowness originally formed by the direction of the layer. Despite the opening of the layer, guided waves in this context would only be observable at stations offshore.

[30] Since the initial slab structure appears oversimplified and unsuited to explain the observations, the slab geometry was adjusted. The modified slab is now smoothly bending downward in the depth range of 90–150 km (hypocenters derived by *Graeber* [1997] and *Rietbrock et al.* [1997]) (see Figure 7). The subduction angle varies from  $16^\circ$  to  $35^\circ$ . A series of snapshots resulting from this enhanced model reveals that the waves are not strictly “guided” by the low-velocity layer but are, in fact, partially transmitted toward the bounding rocks if the structure is not planar (Figure 8). At depth around 100 km, where bending is most severe, part of the energy leaves the low-velocity layer. After the decoupling process, this low-frequency energy proceeds with the same slowness as defined by the lower portion of the slab and same direction through the continental mantle and to the surface.

[31] The slab geometry and alterations in subduction angle, not the local velocity structure of the slab, thus define the point of appearance of guided wave energy at the surface. Within a small stripe around  $140$  km inland from the coastline ( $69.2^\circ\text{W}$ – $68.8^\circ\text{W}$ ) guided waves are observed as  $P$  first arrivals (Figure 7). This is in accordance with the locations of stations AER, BOS, and CHG of the ANCORP network (compare Figure 1).

[32] A receiver at  $69.0^\circ\text{W}$ , where guided wave energy is strongest (see above simulation), illustrates the typical pulse shape of guided waves for down-dip events (Figure 9a). The guided waveforms the low-frequency first arrival that lasts for 1–2 s. The energy trapping effect of the waveguide results in very large amplitudes compared to the higher-frequency body waves which begin to dominate the wave field after around 1 s. The center frequency of the guided wave for the simulated layer thickness comes out to be 2 Hz,

pulse shapes of the synthetics bear similarity to those observed for a focal depth of 200 km (Figure 9b).

#### 4.2.2. Source Depth and Development of Guided Waves

[33] The development of guided waves is controlled by the distance traveled within the low-velocity layer and thus by source depth. To shed some light on the “birth” of a guided wave train, synthetics for different source depths were calculated using the above model (Figure 7). Each synthetic seismogram is displayed together with a recorded signal of the corresponding source depth.

[34] The seismic source is again located within the low-velocity structure to allow an efficient excitation of guided waves. A 7% slow layer as proposed by *Bock et al.* [2000] is assumed. The layer thickness was changed from 3 km in the above tests using the straight slab model to 2 km for the bending slab model. This thickness resulted in the best fits taking into account the reduced propagation distance within the LVL due to the bend in the slab structure and decoupling of guided waves. The source depth varies between 110 and 250 km; accordingly, hypocentral distances range from 140 to 350 km (Figure 10). The receiver remains at  $69^\circ\text{W}$ , where maximum wave amplitudes are observed.

[35] Each of the synthetic seismograms in Figure 10 represents a characteristic pulse form matching the corresponding trace on the observed depth section:

[36] For 110 km focal depth, virtually no guided wave energy is present. Signals travel only a few kilometers within the layer and then decouple when the kink at 100 km depth is reached; therefore no guided waves are excited. Accordingly, no low-frequency peaks are present in spectra of signals originating from source depth less than 110 km. Pulses of synthetics at 200 km focal depth travel along the low-velocity layer for approximately 150 km. The presence of low-frequency guided waves is evident, but at this depth only one to two cycles of the guided wave emerge. Higher frequency energy of phases traversing the lower slab and continental mantle contribute considerably to the waveform. The majority of the observed seismograms at around 200 km source depth bear resemblance to this pattern. Finally, the simulation for 250 km source depth exposes strong low-frequency guided wave energy (Figure 3, bottom). The growing ray path within the layer (230 km) causes more cycles to develop, much like in the observed data for source depth greater than 250 km.

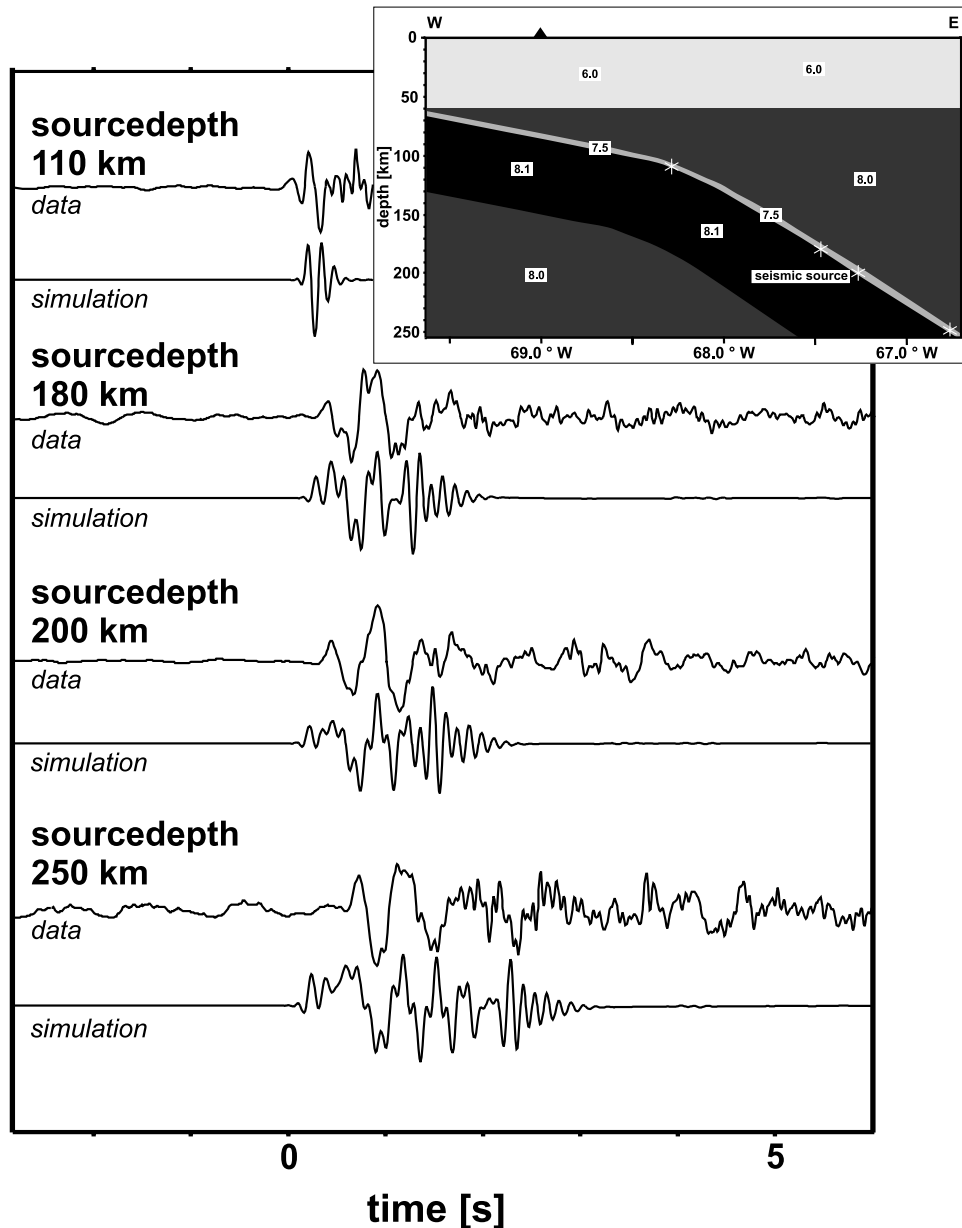


**Figure 10.** Synthetics (receiver at  $69^{\circ}\text{W}$ ) for sources located inside the low-velocity layer (at 0.3 km perpendicular distance to subducted oceanic Moho) at various depths and ANCORP data (recorded at station AER) for the corresponding depths. Signals are aligned using a cross-correlation algorithm. Insert shows the velocity model and source positions.

[37] The observations at different source depth fit well into the scheme of a developing guided wave. As expected, no effect is visible for focal depth above 110 km. Below that depth, guided waves form slowly and become more and more prominent with growing depth.

#### 4.2.3. Waveguide Thickness and Frequency Content of Guided Waves

[38] The model of Figure 7 now serves as a basis for simulations with varying thickness of the low-velocity layer. Source depth is kept constant at 200 km resulting in hypocentral distances comparable to those of observed intermediate depth events (275 km). The layer thickness varies between 1.5 and 7.0 km. Waveforms differ slightly in number of cycles and amplitudes, but the major differences

are in frequency content (Figure 11). Spectra of the first 2 s of the signals underline the tendency toward higher frequencies for thinner layers. Layers of average width greater than 4.5 km do not yield strong low-frequency guided wave energy in the relevant frequency region. The spectrum of the 7 km thick LVL, for example, is clearly dominated by a high-frequency peak resulting from direct  $p$  waves arriving in the same time window as the guided waves. Thus there is evidence that only a fraction of the former crust functions as a low-velocity wave guide. This is in accordance with studies at comparable depth for other slabs [Helffrich, 1996].

[39] Layer thickness is coupled more than any other waveguide parameter with frequency content of the guided

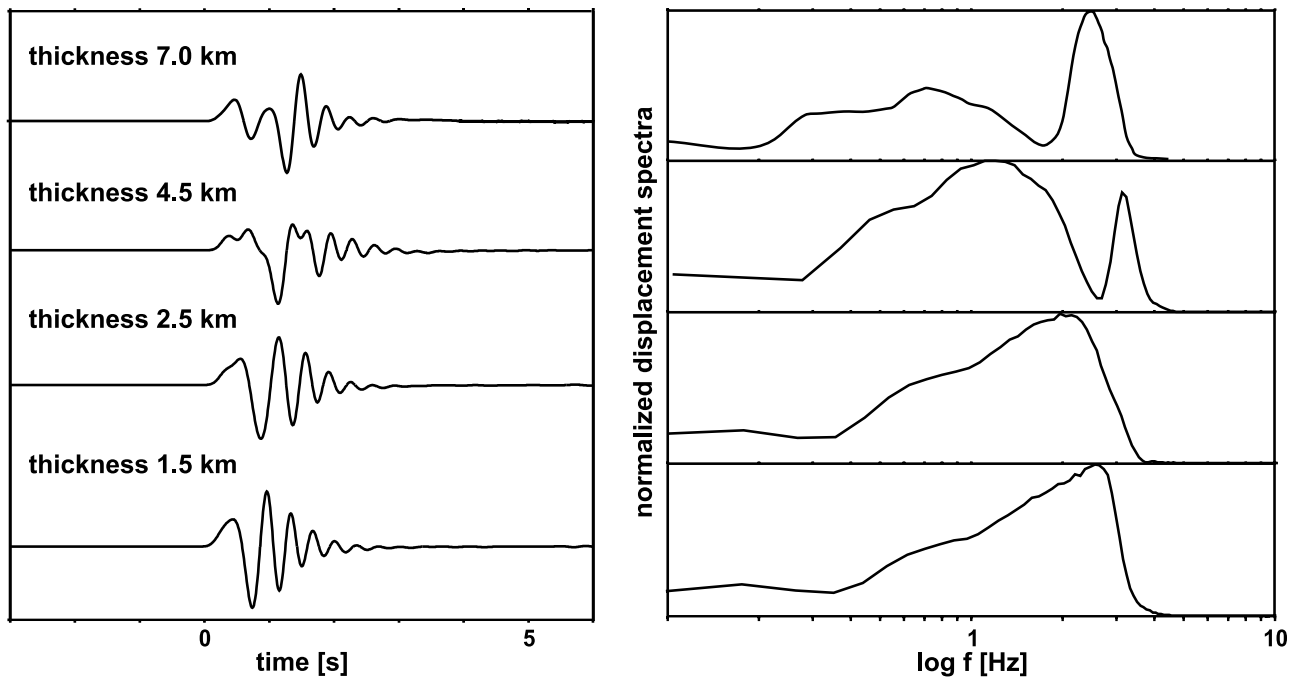


**Figure 11.** Synthetics and spectra for low-velocity layers of varying thickness (velocity model, see insert of Figure 7). Source depth is 200 km, and seismograms are low-pass-filtered (3 Hz) to emphasize the low-frequency guided waves.

waves. On the other hand, estimation of thickness of subducted low-velocity crust is by no means straight forward. A number of other factors are known to produce frequency shift of the waves, namely, propagation distance within the layer, velocity contrasts, and attenuation effects [Ben-Zion, 1998].

[40] Taking into account constraints given by the possible mineralogical regimes, the variation in velocity is restricted to 5–15% (untransformed gabbro) [e.g., Helffrich and Stein, 1993]. Variations within this range yield only marginal changes in the spectral content of the signals. Quality factors within the cold subducted crust are higher than 400 as imaged by Haberland and Rietbrock [2001]; however, dehydration processes may locally cause high attenuation.

#### 4.2.4. Guided Waves and Source Location

[41] The appearance of guided waves is of course dependent on the source location relative to the waveguide [e.g., Li and Vidale, 1996]. Thus the waveguide effect may constrain two major aspects of the subduction process. The guided wave observations (1) have potential to put constraints on localization of hypocenters on a much smaller scale than possible even by 3-D location algorithms so far and (2) may help to determine up to which depth range oceanic crust persists and whether a complete eclogite transformation takes places. The following tests throw light on the sensitivity of the observed waveform to source location relative to the low-velocity layer.

[42] Unlike assumed until recently, guided waves may, under certain conditions, also be excited by sources located outside the low-velocity layer [Abers, 2000; Fohrmann et al., submitted manuscript, 2002]. A first exemplary test was carried out for a source at 200 km focal depth located below the low-velocity layer at a perpendicular distance of 7 km.

Apparently, only little energy enters the layer (Figure 12), and the waveguide effect is much less intense for sources located outside the structure. Moreover, emergent body wave phases now mask the guided wave energy,  $P$  onsets are dominated by rather high frequencies and do not resemble the observations. Considering attenuation and scattering present in the data, the low-frequency energy would probably be drowned out by the coda of  $P$  waves traveling within the faster slab.

[43] The second issue connected to source location to be addressed here is the compatibility of our interpretation of the low-frequency onsets with a possible breakdown and transformation of the oceanic crust at depths in the range of 80–200 km [Fukao et al., 1983; Hori et al., 1985; Helffrich et al., 1989]. If a complete transformation of gabbroic crust into eclogite at intermediate depth takes place, the layer of reduced velocity would be transformed into a high-velocity channel. Sources of deep events would then be situated in the continuation of the low-velocity subducted crust but at several tens of kilometers distance beneath it. It is thus of special interest, whether the observed guided waves for focal depth greater than 160 km can be caused by a low-velocity layer that exists only down to depth of 160 km (the maximum extend of layering inferred so far for the Chile-Peru subduction zone [Bock et al., 2000]). The modified model in Figure 13 depicts this situation.

[44] Synthetics for different focal depths for a layer that diminishes below 160 km depth are displayed in Figure 13 (receiver position is 69°W). The simulated  $P$  onsets are in accordance with the observations, high-amplitude low-frequency energy arrives prior to higher frequencies (Figure 13). This means that the waveguide also influences signals from sources located near the slab surface in continuation of the former low-velocity subducted crust. Simulations

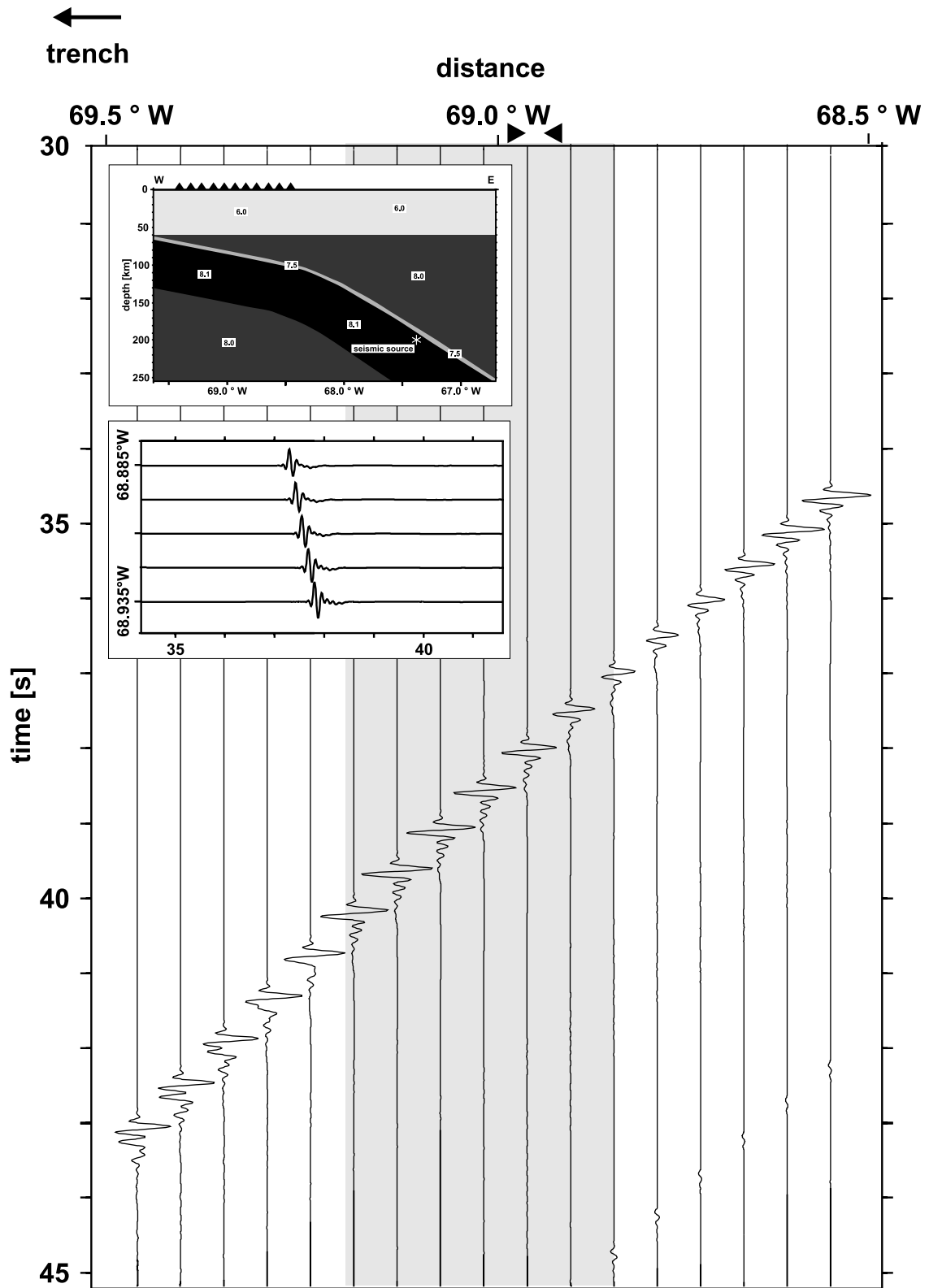


**Figure 12.** Seismogram section for a source located 7 km below the subducted crust. Source depth is 200 km. Top insert is the velocity model. Bottom insert shows enlargement of receivers located around 68.9°W (station AER).

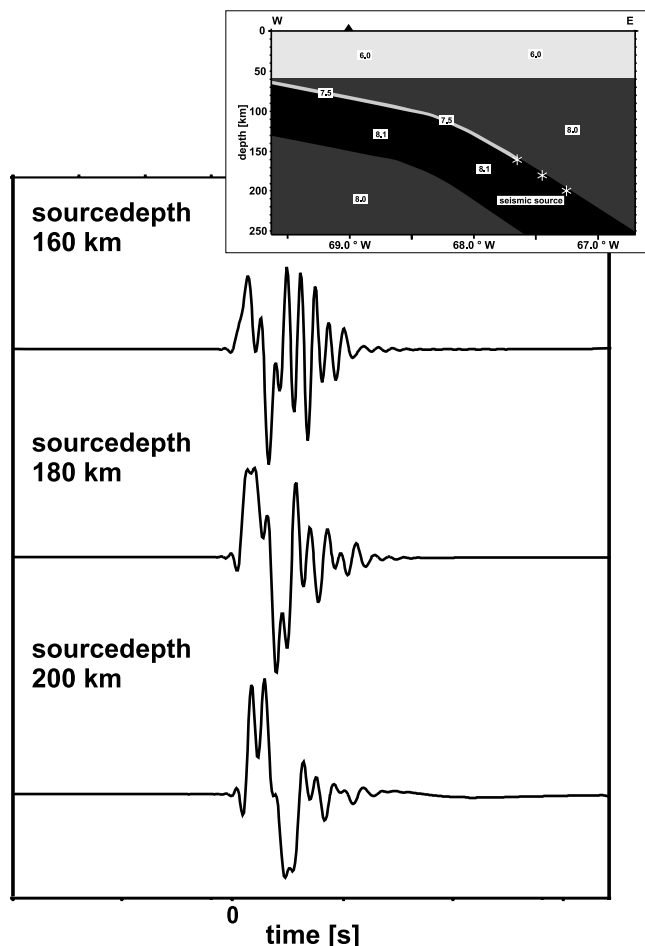


**Figure 13.** Seismograms for sources located beneath the low-velocity subducted crust. The low-velocity layer ends at 160 km depth. Sources are at 1.2 km perpendicular distance to the slab surface. Insert shows the velocity model.

with sources located more than 10 km away from the slab surface fail to produce guided wave energy (not shown). This possibly indicates that deep sources registered in the ANCORP campaign are located in continuation of the already transformed low-velocity structure, while events at intermediate depth are located inside the layer.

## 5. Conclusion

[45] We summarize our results on the basic issues of (1) slab geometry and decoupling of guided waves, (2) source position and excitation of guided waves, and (3) layer thickness and frequency content.

### 5.1. Decoupling of Guided Waves

[46] Remarkably, we are able to observe guided waves at receivers well outside of the waveguide (distances around 100 km) and are thus provided with information on waveguide structures located at greater depth. In contrast, most waveguide studies for the Japanese slab and works on fault zones investigate primarily more or less shallow waveguides where receivers are situated directly above the structure [Fukao et al., 1983; Hori, 1990; Ben-Zion et al.,

2003]. We focus on updip events, studies at other subduction zones reported similar waves using along-strike data [Ansell and Gubbins, 1986; Matsuzawa et al., 1987; Abers, 2000]. The updip geometry provides unique information on the decoupling process of the guided waves.

[47] Within the subduction zone context, guided waves are observed only at certain receiver locations and not necessarily close to the coast line. Their point of occurrence is determined by the shape and geometry of the surface of subducted lithosphere. The average dip of the low-velocity layer determines the slowness and ultimately the point of occurrence of guided waves at the free surface. At the Chile Peru subduction zone, the dip angle of approximately  $36^\circ$  at intermediate depth defines the point of appearance of guided waves at  $68.9^\circ\text{W}$ .

[48] This restricts fast guided energy causing distorted  $P$  onsets at the investigated site to a small stripe centered around  $69.8^\circ\text{W}$  paralleling the strike of the subducted slab. Data of the PISCO'94 network located farther south ( $24^\circ\text{S}$ ) also exposes low-frequency onsets for receiver locations in accordance with our model. We are confident to observe and utilize similar effects at other subduction zones, provided that data from sections with small receiver spacing perpendicular to the strike are available.

### 5.2. Source Location

[49] The observed waveguide effect constrains source locations relative to the layer. Our study confirmed that the effect does virtually not occur for sources located in the subducted slab outside a continuous low-velocity layer. Thus there is evidence that intraslab events with focal depth down to approximately 160 km are located within a few kilometers of the layer, a finding already proposed at other subduction zones so far [Matsuzawa et al., 1986; Abers, 2000].

[50] However, our results do not imply that all source locations are restricted to within such a thin layer at the top of the slab surface. Simulations indicate that sources situated beneath a finite low-velocity layer can still produce the effect, if they are located in continuation of the structure (i.e., near the slab surface). To draw sound conclusions, however, further detailed investigations are needed. In particular, source mechanisms other than explosive sources have to be tested. Then source locations relative to the slab surface can potentially be restricted for given event depths and ultimately, inferences on the depth of breakdown of the low-velocity layer will be possible.

### 5.3. Waveguide Thickness

[51] The frequency content of observed guided waves is a strong function of the average thickness of the structure. Comparison of finite difference simulations with the data recorded at station AER of the ANCORP network show that velocity contrasts of metastable gabbro (7% low velocity) result in very promising pulse shapes for a layer thickness of 2 km (compare Figure 10). Damping effects that were not considered in the elastic simulations may influence the layer thickness [Ben-Zion, 1998]. However, attenuation leads to an overestimation of the layer thickness. Thus our estimates are representing upper limits for layer thickness. Simulations give strong evidence that below 100 km depth a layer of 7 km average thickness (i.e., the width of the subducted

oceanic crust) can not be reconciled with the data, even a layer of 5 km width can neither match the 2 Hz frequency peak present in the data nor excite sufficient guided waves (see Figure 11).

#### 5.4. Consequences for the Subducting Nazca Plate

[52] Our findings show that the observed frequency effect is caused by guided waves developing in a thin low-velocity layer located in the continental mantle beneath northern Chile at 21°S. The part of the low-velocity structure illuminated by guided waves is situated at depth greater than 100 km. It resembles a rather thin layer (<4.5 km) of 7% low velocity at the slab surface reaching down to depth of 160 km, probably further. We therefore conclude that we do not image an untransformed basaltic oceanic crust (which we expect to be thicker) but a low-velocity layer that results from mineralogical phase changes taking place within or in the vicinity of the former subducted crust at the interface between continental mantle and subducted lithosphere. For comparable depth, studies at other subduction zones have so far found evidence for a similar low-velocity region [Matsuzawa *et al.*, 1987; Abers and Sarker, 1996; Helffrich and Abers, 1997; Abers, 2000]. Possible compositions for such a layer have been suggested, e.g., by Helffrich [1996], Peacock [1996], and Hacker *et al.* [2003a, 2003b].

[53] Our results regarding the Chile-Peru subduction zone seem to agree with the latest mineralogical model proposed by Hacker *et al.* [2003a, 2003b]. In this scheme, subducted crust in the depth range of interest is depicted as a coarse grained, partially eclogized low-velocity layer (the lower crust) topped by dehydrated upper crust. From the simulated layer width for the Chile-Peru slab, we deduce that the guided waves image the slow, lower part of subducted crust at intermediate depth. Whether or not this interpretation is to be favored among the other possible mineral assemblages requires further research. In any case, the waveguide is a persistent feature of the subducted Nazca slab and the Chile-Peru subduction zone is one more example within the Pacific subduction zones that features a low-velocity layer at the top of the slab surface extending to depths of 100–160 km.

[54] **Acknowledgments.** Thanks are due to the members of the Cluster Computing Group of the Institut für Informatik (Universität Potsdam) for their support and resources on the LINUX cluster. ANCORP and PISCO experiments were financed by the German Science Foundation (DFG) through the SFB 267, the GeoForschungsZentrum Potsdam (GFZ), and the Free University of Berlin (FUB). GIPP (GFZ) and FUB provided the instruments.

#### References

- Abers, G. A., Hydrated subducted crust at 100–250 km depth, *Earth Planet. Sci. Lett.*, 176, 323–330, 2000.
- Abers, G. A., and R. Sarker, Dispersion of regional body waves at 100–150 km depth beneath Alaska: in situ constraints on metamorphism of subducted crust, *Geophys. Res. Lett.*, 23, 1171–1174, 1996.
- ANCORP Working Group, Seismic reflection image revealing offset of Andean subduction-zone earthquake locations into oceanic mantle, *Nature*, 397, 341–344, 1999.
- Ansell, J. H., and D. Gubbins, Anomalous high-frequency wave propagation from the Tonga-Kermadec seismic zone to New Zealand, *Geophys. J. R. Astron. Soc.*, 85, 93–106, 1986.
- Barazangi, M. B., B. Isacks, and J. Oliver, Propagation of seismic waves through and beneath the lithosphere that descends under the Tonga island arc, *J. Geophys. Res.*, 77, 952–958, 1972.
- Ben-Zion, Y., Properties of seismic fault zone waves and their utility for imaging low velocity structures, *J. Geophys. Res.*, 103, 12,567–12,585, 1998.
- Ben-Zion, Y., Z. Peng, D. Okaya, L. Seeber, J. G. Armbruster, N. Ozer, A. J. Michael, S. Baris, and M. Aktar, A shallow fault zone structure illuminated by trapped waves in the Karadere-Duzca branch of the North Anatolian Fault, western Turkey, *Geophys. J. Int.*, 152(3), 699–717, 2003.
- Bock, G., B. Schurr, and G. Asch, High-resolution image of the oceanic Moho in the subducting Nazca plate from P-S converted waves, *Geophys. Res. Lett.*, 27, 3929–3932, 2000.
- Davies, D., and D. P. McKenzie, Seismic travel-time residuals and plates, *Geophys. J. R. Astron. Soc.*, 18, 51–63, 1969.
- Fukao, Y., K. Kanjo, and I. Nakamura, Deep seismic zone as an upper mantle reflector of body waves, *Nature*, 272, 606–608, 1978.
- Fukao, Y., S. Hori, and M. Ukawa, A seismological constraint on the depth of basalt-eclogite transition in a subducting oceanic crust, *Nature*, 303, 413–415, 1983.
- Graeber, F. M., Seismische Geschwindigkeiten und Hypozentren in den Südlichen Zentralen Anden aus der simultanen Inversion von Laufzeitdaten des seismologischen Experiments PISCO '94 in Nordchile, Ph.D. thesis, GeoForschungszentrum Potsdam, Germany, 1997.
- Haberland, C., and A. Rietbrock, Attenuation tomography in the western central Andes: A detailed insight into the structure of a magmatic arc, *J. Geophys. Res.*, 106, 11,151–11,167, 2001.
- Hacker, B. R., S. M. Peacock, G. A. Abers, and S. D. Holloway, Subduction factory, 1, Theoretical mineralogy, densities, seismic wave speeds and H<sub>2</sub>O contents, *J. Geophys. Res.*, 108(B1), 2029, doi:10.1029/2001JB001127, 2003a.
- Hacker, B.R., S. M. Peacock, G. A. Abers, and S. D. Holloway, Subduction factory, 2, Are intermediate-depth earthquakes in subducting slabs linked to metamorphic dehydration reactions?, *J. Geophys. Res.*, 108(B1), 2030, doi:10.1029/2001JB001129, 2003b.
- Helffrich, G., Subducted lithospheric slab velocity structure: Observations and mineralogical inferences, in *Subduction Top to Bottom*, *Geophys. Monogr. Ser.*, vol. 96, edited by G. E. Bebout *et al.*, pp. 215–222, AGU, Washington, D. C., 1996.
- Helffrich, G., and G. A. Abers, Slab low-velocity layer in the eastern Aleutian subduction zone, *Geophys. J. Int.*, 130, 640–648, 1997.
- Helffrich, G. R., and S. Stein, Study of the structure of the slab mantle interface using reflected and converted seismic waves, *Geophys. J. Int.*, 115, 15–40, 1993.
- Helffrich, G., S. Stein, and B. J. Wood, Subduction zone thermal structure and mineralogy and their relationship to seismic wave reflections and conversions at the slab/mantle interface, *J. Geophys. Res.*, 94, 753–763, 1989.
- Hori, S., Seismic waves guided by untransformed oceanic crust subducting into the mantle: The case of the Kanto district, central Japan, *Tectonophysics*, 176, 355–376, 1990.
- Hori, S., H. Inoue, Y. Fukao, and M. Ukawa, Seismic detection of the untransformed basaltic oceanic crust subducting into the mantle, *Geophys. J. R. Astron. Soc.*, 83, 169–197, 1985.
- Hurukawa, N., and M. Imoto, Subducting oceanic crusts of the Phillipine Sea and Pacific Plates, *Geophys. J. Int.*, 109, 652–693, 1992.
- Igel, H., Y. Ben-Zion, and P. C. Leary, Simulation of SH- and P-SV-wave propagation in fault zones, *Geophys. J. Int.*, 128, 533–546, 1997.
- Iidaka, T., and K. Obara, The upper boundary of the subducting pacific plate estimated from ScSp waves beneath the Kanto region, Japan, *J. Phys. Earth*, 41, 103–108, 1993.
- Kirby, S., E. R. Engdahl, and R. Denlinger, Intermediate-depth intraslab earthquakes and arc volcanism as physical expressions of crustal and uppermost mantle metamorphism in subducting slabs, in *Subduction Top to Bottom*, *Geophys. Monogr. Ser.*, vol. 96, edited by G. E. Bebout *et al.*, pp. 195–214, AGU, Washington, D. C., 1996.
- Lessel, K., Die Krustenstruktur der zentralen Anden in Nordchile (21–24°S), abgeleitet aus 3D-Modellierungen refraktionsseismischer Daten, Ph.D. thesis, Freie Univ., Berlin, Germany, 1997.
- Levander, A. R., Fourth order finite difference P-SV-seismograms, *Geophysics*, 53, 1425–1436, 1988.
- Li, Y.-G., and P. C. Leary, Fault zone trapped waves, *Bull. Seismol. Soc. Am.*, 80, 1245–1271, 1990.
- Li, Y.-G., and J. E. Vidale, Low-velocity fault-zone guided waves: Numerical investigations of trapping efficiency, *Bull. Seismol. Soc. Am.*, 86, 371–378, 1996.
- Matsuzawa, T., N. Umino, A. Hasegawa, and A. Takagi, Upper mantle velocity structure estimated from PS-converted wave beneath the northeastern Japan Arc, *Geophys. J. R. Astron. Soc.*, 86, 767–787, 1986.
- Matsuzawa, T., N. Umino, A. Hasegawa, and A. Takagi, Estimation of thickness of a low-velocity layer at the surface of the descending oceanic plate beneath the northeastern Japan arc by using synthesized PS-wave, *Thoku Geophys. J.*, 31, 19–28, 1987.

- Meade, C., and R. Jeanloz, Deep-focus earthquakes and recycling of water into the Earth's mantle, *Science*, 252, 68–71, 1991.
- Mitronovas, W., B. L. Isacks, C. Meade, and R. Jeanloz, Seismic velocity anomalies in the upper mantle beneath the Tonga-Kermadec island arc, *J. Geophys. Res.*, 76, 7154–7180, 1971.
- Oda, H., T. Tanaka, and K. Seya, Subducting oceanic crust on the Philippine Sea Plate in southwest Japan, *Tectonophysics*, 172, 175–189, 1990.
- Patzwahl, R., Plattengeometrie und Krustenstruktur am Kontinentalrand Nord-Chiles aus weitwinkelseismischen Messungen, Ph.D. thesis, Freie Univ., Berlin, Germany, 1998.
- Peacock, S. M., Thermal and petrological structure of subduction zones, in *Subduction Top to Bottom*, *Geophys. Monogr. Ser.*, vol. 96, edited by G. E. Bebout et al., pp. 119–133, AGU, Washington, D. C., 1996.
- Randal, C. J., Absorbing boundary condition for the elastic wave equation: Velocity stress formulation, *Geophysics*, 54, 1141–1152, 1989.
- Rietbrock, A., G. Asch, G. Chong, and P. Giese, ANCORP '96—Seismicity along the ANCORP traverse in northern Chile, *Eos Trans. AGU*, 78(46), Fall Meet. Suppl., F716, 1997.
- Snoke, J. A., I. S. Sacks, and H. Okada, Determination of the subducting lithosphere boundary by use of converted phases, *Bull. Seismol. Soc. Am.*, 67, 1051–1060, 1978.
- Van der Hilst, R., and R. Snieder, High-frequency precursors to p wave arrivals in New Zealand: Implications for slab structure, *J. Geophys. Res.*, 101, 8473–8488, 1996.
- Virieux, J., *SH*-wave propagation in heterogeneous media: Velocity stress finite difference method, *Geophysics*, 49, 1933–1957, 1984.
- Virieux, J., *P-SV*-wave propagation in heterogeneous media: Velocity stress finite difference method, *Geophysics*, 51, 889–901, 1986.
- Yuan, X., S. V. Sobolev, R. Kind, O. Oncken, and A. S. Group, Subduction and collision processes in the central Andes constrained by converted seismic phases, *Nature*, 408, 958–961, 2000.

---

G. Asch and C. Haberland, GeoForschungszentrum Potsdam, Telegrafenberg E254, D-14473 Potsdam, Germany. (asch@gfz-potsdam.de; haber@gfz-potsdam.de)

S. Martin, Institut für Geowissenschaften, Universität Potsdam, Karl-Liebknecht-Str. 24/H25, D-14476 Golm, Germany. (smartin@geo.uni-potsdam.de)

A. Rietbrock, Department of Earth and Ocean Sciences, University of Liverpool, Jane Herdman Laboratories, 4 Brownlow Street, Liverpool L69 3GP, UK. (ariet@liv.ac.uk)